J Mater Sci: Mater Electron (2015) 26:2987–2994
DOI 10.1007/s10854-015-2787-8

Molten salt synthesis and tunable photoluminescent properties of Eu^{3+}–Tb^{3+} doped $NaY(MoO_4)_2$ microcrystals

Xue Zhang · Yunfei Liu · Yinong Lu · Bingyan Li · Fei Song · Fengling Yang

Received: 11 October 2014 / Accepted: 31 January 2015 / Published online: 8 February 2015

Abstract Octahedron-like and rod-like $NaY(MoO_4)_2$ microcrystals with tetragonal scheelite-type structure were successfully synthesized by a low cost molten salt method using NaCl as the reaction medium. The as-obtained products were characterized by powder X-ray diffractometer, thermal field emission scanning electron microscope, and photoluminescence spectrometer. The results show that $NaY(MoO_4)_2$ with different morphologies have been controllably obtained via adjusting calcining temperature and reaction time. Under the UV light excitation, the emission intensity of the octahedron-like $NaY(MoO_4)_2$:Eu^{3+}/Tb^{3+} microcrystals is stronger than the rod-like ones. Moreover, the luminescence colors of the Eu^{3+}–Tb^{3+} co-doped $NaY(MoO_4)_2$ octahedron-like microcrystals can be tuned from red, orange, yellow and green-yellow to green by simply adjusting the relative doping concentrations of the activator ions, which might have potential application in the areas such as optoelectronic devices in the future.

1 Introduction

As far as we concerned, the physicochemical properties of inorganic functional materials depend on not only the chemical composition, structure and crystal phase but also the morphology factors, including shape, size and dimensionality [1–3]. Therefore, research efforts have focused on developing convenient and efficient approaches for the manufacture of various luminescent materials with tunable microstructures as well as different shapes and sizes [4–6].

Double alkaline rare earth tungstates and molybdates [$ALn(MO_4)_2$, where A is an alkali-metal cation, Ln is a rare earth metal cation, M is Mo^{6+} or W^{6+}] can generate various inorganic compounds having tetragonal and monoclinic symmetries, which have been considered as promising host materials for doping with rare earth ions [7–9]. $ALn(MO_4)_2$ have been widely used in various areas such as optoelectronic device, flat plane display and biological imaging [10, 11], by virtue of their sharp emission lines, high mono-chromaticity, long luminescence life-time and high photo-stability [12–14]. Besides, they can be used to prepare all kinds of phosphors that emit a variety of colors by doping different lanthanide ions [15–17].

Recently, several molybdate micro/nano materials have been obtained by many synthesis techniques such as solid state method, molten salt method, hydrothermal or solvothermal method and template method. $NaY(MoO_4)_2$ with different morphologies have been synthesized successfully by a hydrothermal method [18–20]. The molten salt method, providing the advantage of simple instrumentation, easy manipulation and effective cost, is available for obtaining purified, crystalline, single-phase powders at a lower temperature [21, 22]. On the basis of the advantages of molten salt method for chemical synthesis of micro/nanocrystals, Yan et al. synthesized sphere-like $ZnWO_4$:Eu^{3+} powders [23], which presented the homogenous nanometer particle size. And Wu et al. [24] prepared large-scale 1D rod-like $KEu(MoO_4)_2$ microcrystals. Nowadays, the materials emitting multiple colors have become a research focus because of their important role in

X. Zhang · Y. Liu (✉) · Y. Lu (✉) · B. Li · F. Song · F. Yang
State Key Laboratory of Materials-Oriented Chemical Engineering, College of Materials Science and Engineering, Nanjing Tech University, Nanjing 210009, China
e-mail: yfliu@njtech.edu.cn

Y. Lu
e-mail: yinonglu@njtech.edu.cn

some fields such as large screen electrical display devices [10]. Zeng et al. [25] co-doped $Gd_2(WO_4)_2$ microstars with different amounts of Eu^{3+} and Tb^{3+} giving rise to a variety of colors including warm-white light. Urchin-like $NaY(MoO_4)_2$ microarchitectures synthesized by a hydrothermal process were also co-doped with Eu^{3+} and Tb^{3+} (to a total concentration of 5 %) by Xu et al. [19].

In this paper, molten salt synthesis technology has been engaged in the synthesis of $NaY(MoO_4)_2$ microcrystals in the NaCl medium at different reaction parameters. The morphology of the $NaY(MoO_4)_2$ was found to be manipulated by changing the calcining temperature and reaction time. Furthermore, the luminescence properties of Eu^{3+}/Tb^{3+} doped $NaY(MoO_4)_2$ and the tunable emission of Eu^{3+}–Tb^{3+} co-doped $NaY(MoO_4)_2$ have also been investigated.

2 Experimental

2.1 Preparation of samples

Starting chemicals (Na_2CO_3, MoO_3, Y_2O_3, Eu_2O_3, Tb_4O_7, NaCl) purchased from Shanghai Chemical Reagents Co. Ltd. were of analytical reagent grade and used as received without further purification. Tb_2O_3 was prepared under reducing atmosphere of hydrogen for 12 h at 900 °C with Tb_4O_7 as the reactant. In order to synthesize $NaY(MoO_4)_2$ microcrystals, the reactants Na_2CO_3, Y_2O_3 and MoO_3 (molar ratios of 1:1:4) were mixed with 40 wt% NaCl medium in absolute ethanol by ball milling for 7 h, and then calcined at 650–850 °C with the heating rate of 10 °C min^{-1} for 0.5–10 h in an alumina crucible. The as-prepared products were washed thoroughly with deionized water several times until no free chloride ions were detected by the $AgNO_3$ solution. Finally, the obtained products were dried at 80 °C for 24 h and kept for further characterization. Eu^{3+}/Tb^{3+} doped and co-doped $NaY(MoO_4)_2$ microcrystals were prepared in a similar way.

2.2 Characterization

The phase structure of the as-prepared products was identified by powder X-ray diffractometer (XRD, SmartLab-3kw, Rigaku Ltd, Japan) using Cu Ka radiation at a scanning rate of 5° min^{-1} in a 2θ range of 5–80°. The thermal field emission scanning electron microscope (FE-SEM, Ultra55, ZEISS, German) was employed for the observation of the morphology and size of the products. The X-ray room temperature PL spectra were recorded on FL3-221 fluorescence spectrometer (HORIBA Jobin-Yvon, France).

3 Result and discussion

3.1 Phase and morphology

The XRD patterns of $NaY(MoO_4)_2$ powders obtained at 650–850 °C for 6 h in the presence of NaCl medium are shown in Fig. 1. All diffraction peaks of the as-obtained white powders can be readily indexed to the pure tetragonal phase of $NaY(MoO_4)_2$ [space group: I41/a (88)] according to the JCPDS Card No. 52-1802. The strong and sharp diffraction peaks indicate the high crystallinity of the synthesized products, and no additional peaks of other phases can be found, revealing a high purity of the obtained powders. Evidences above indicate that well-crystallized tetragonal $NaY(MoO_4)_2$ crystals are obtained under the present molten salt conditions at 650 °C and above.

The calcining temperature plays an important role in the final morphology and size of the products as shown in Fig. 2. At 650 °C, the products consist of some small particles and rod-like microcrystals (Fig. 2a). The products obtained at 700 °C are composed of rod-like morphologies with an average dimension of 300–600 nm in length and 100 nm in diameter as well as some small particles (Fig. 2b). When the calcining temperature increases to 750 °C (Fig. 2c), the quantities of rod-like crystals decrease and octahedral-like particles preliminary generate. After the calcining temperature increases to 800 °C (Fig. 2d), the products are mainly uniform octahedral-like $NaY(MoO_4)_2$ particles with an average size of 200–500 nm, leaving almost no rod-like crystals. When the calcining temperature reaches to 850 °C, some larger particles with irregular morphology generate,

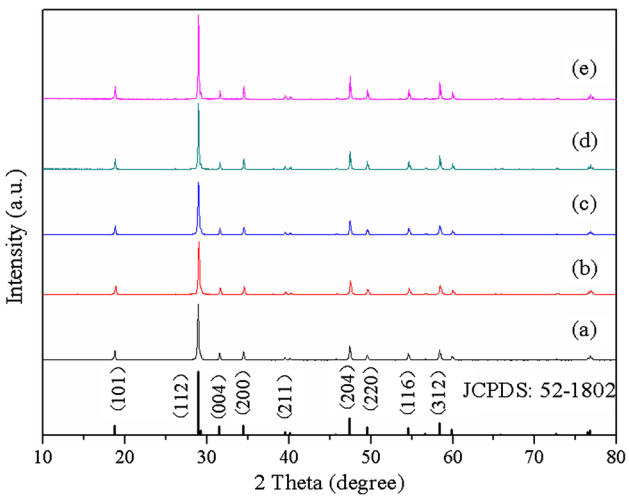

Fig. 1 XRD patterns of the $NaY(MoO_4)_2$ obtained at different calcining temperatures for 6 h: (*a*) 650 °C, (*b*) 700 °C, (*c*) 750 °C, (*d*) 800 °C, (*e*) 850 °C. The standard pattern of tetragonal $NaY(MoO_4)_2$ (JCPDS 58-1802) is also presented at the *bottom* for comparison

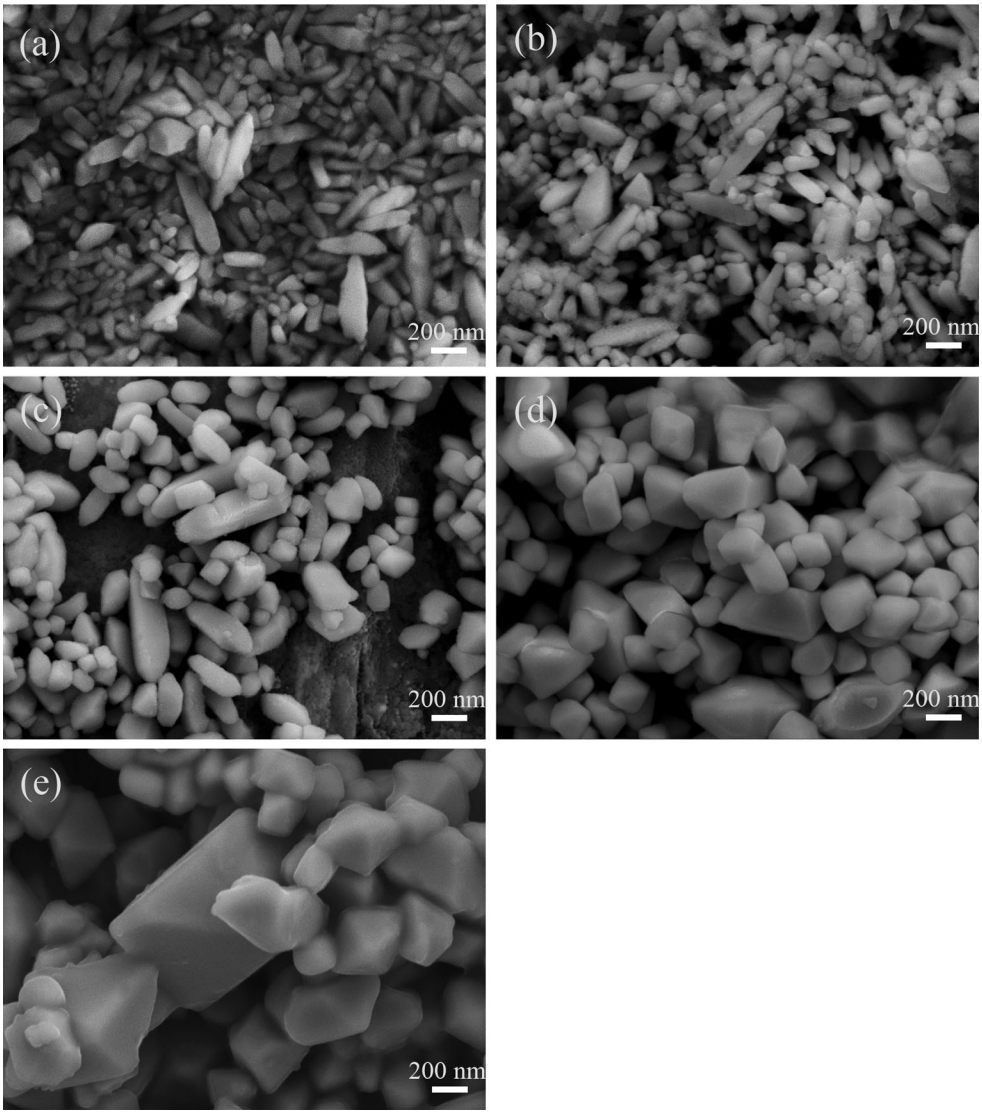

Fig. 2 FE-SEM images of the $NaY(MoO_4)_2$ obtained at different calcining temperatures for 6 h: **a** 650 °C, **b** 700 °C, **c** 750 °C, **d** 800 °C, **e** 850 °C

these large particles give birth to an inhomogeneous grain distribution of the products (Fig. 2e).

The molten medium is able to promote the effective collision between the small micro/nanoparticles, contributing to the growth of the crystals and inducing the formation of new crystallographic faces on them [26]. In this paper, the melting point of NaCl using as medium is around 800 °C. When the reaction temperature is below 800 °C, the small size particles do not have effective collision between each other because that NaCl medium can not provide a fluid environment for the reactants. Therefore, the length direction becomes the preferential growth direction, which results in forming the rod-like $NaY(MoO_4)_2$ crystals. When the calcining temperature reaches to 800 °C, a highly supersaturated solution [27] is formed and the effective collision becomes active for the reason that the temperature is closed to the melting point of NaCl medium. As a result, the new octahedron-like $NaY(MoO_4)_2$ particles generate because of the same effective collision rate in each direction.

Furthermore, the time-dependent experiments were conducted by keeping the other synthetic parameters remaining unchanged, including the calcining temperature, the weight of molten salt and the heating rate. The XRD patterns of $NaY(MoO_4)_2$ crystals synthesized using NaCl molten salt at 800 °C for different reaction times: (a) 0.5 h, (b) 2 h, (c) 6 h and (d) 10 h are compared (Fig. 3). The tetragonal phase structure of the $NaY(MoO_4)_2$ remains when the reaction time is controlled in the range from 0.5 to 10 h. The XRD results reveal that pure scheelite-type

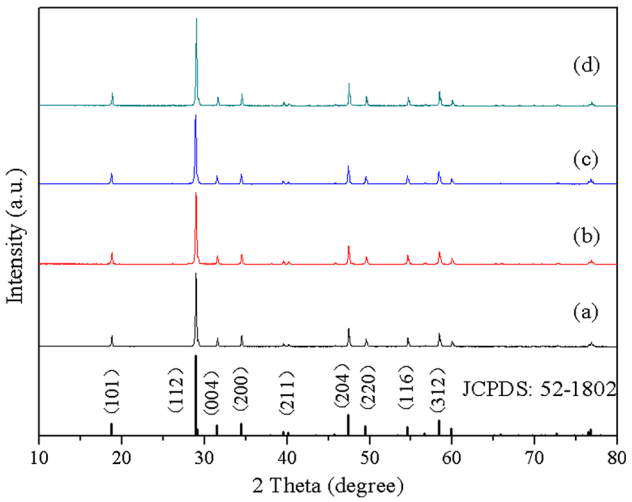

Fig. 3 XRD patterns of the $NaY(MoO_4)_2$ obtained at 800 °C for different reaction times: (*a*) 0.5 h, (*b*) 2 h, (*c*) 6 h, (*d*) 10 h. The standard pattern of tetragonal $NaY(MoO_4)_2$ (JCPDS 58-1802) is also presented at the *bottom* for comparison

$NaY(MoO_4)_2$ crystals could be formed by molten salt method even suffering a short reaction time (0.5 h).

Figure 4 presents the FE-SEM images of the tetragonal phase $NaY(MoO_4)_2$ crystals obtained at 800 °C for different reaction time. With the reaction time of 0.5 h, tiny particles aggregate together into bulks due to the small dimensions and high surface energy (Fig. 4a). With the reaction time of 2 h (Fig. 4b), the products are mainly octahedron-like $NaY(MoO_4)_2$ crystals with the size of 100–300 nm and some small size particles. When the reaction time is prolonged to 6 h, the $NaY(MoO_4)_2$ crystals have narrow particle size distribution and an average size of 200–500 nm (Fig. 4c). When the reaction carries out for 10 h, some other morphologies appear and the products have a broad size distribution (Fig. 4d).

The relevant formation mechanism of different double alkaline rare earth tungstates and molybdates has been reported several times in the literature. For example, Liu et al. [18] revealed that the bipyramid-like $NaY(MoO_4)_2$ microcrystals were formed by a three-step ''dissolution–renucleation–growth'' mechanism. Nowadays, the oriented aggregation and preferential growth mechanisms also have been successfully proposed to explain the formation of octahedron-like microcrystals [28]. The well-known Ostwald ripening, in which small crystallites such as ions, atoms, or molecules grow into larger ones, is generally believed to be the main path of crystal growth [18, 29].

On the basis of the above morphological evolution, an oriented aggregation and Ostwald ripening progress can be proposed for the formation of octahedron-like $NaY(MoO_4)_2$ crystals. The reactants initially begin to fuse into the ion state with the rise of the reaction temperature in the presence of NaCl molten salt. The mixing of Na^+, Y^{3+} and MoO_4^{2-} ions results in the direct formation of

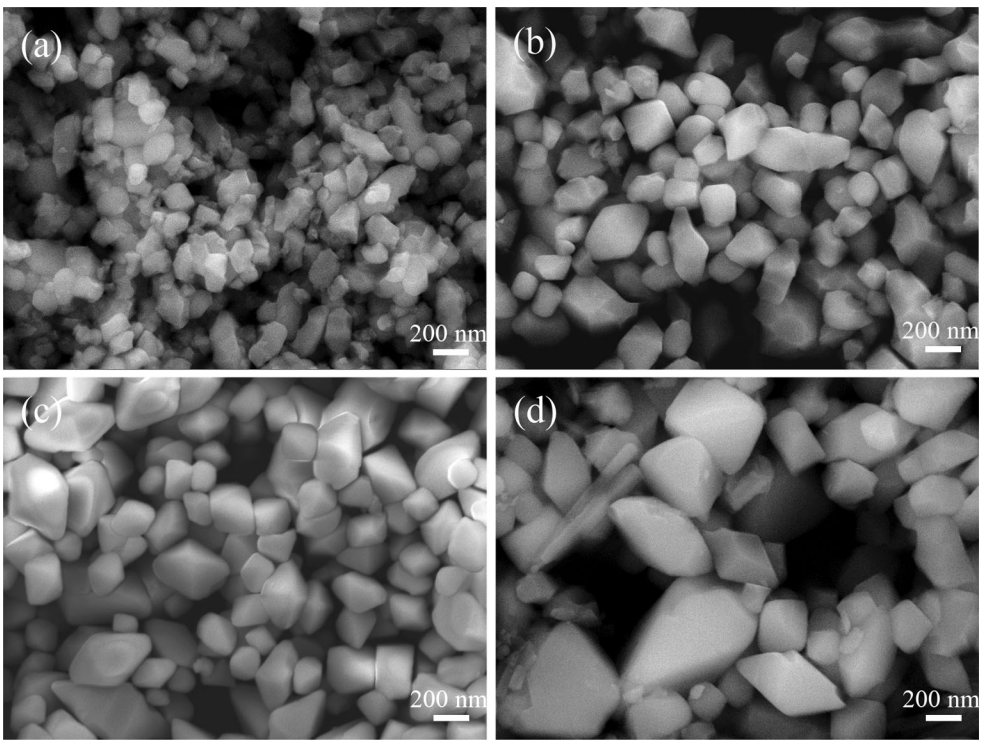

Fig. 4 FE-SEM images of the $NaY(MoO_4)_2$ obtained at 800 °C for different reaction times: **a** 0.5 h, **b** 2 h, **c** 6 h, **d** 10 h

$NaY(MoO_4)_2$ nuclei. With the presence of molten salt, Cl^- can be absorbed to the surfaces of growing particles, which promotes the formation of amorphous $NaY(MoO_4)_2$ nanoparticles and reduces energy consumption. And then, part of the nucleation clusters aggregate together into some tiny octahedral-like microparticles which have unstable facets with relatively high surface energy. The reason for above phenomenon is that the formation of octahedral-like microparticles can greatly reduce the interfacial energy of primary amorphous particles. At the last stage, larger octahedron-like $NaY(MoO_4)_2$ crystals eventually generate at the cost of the small ones according to the typical Ostwald ripening process. And Cl^- can be desorbed from the surfaces of the $NaY(MoO_4)_2$ crystals due to the desorption efficiency [24].

3.2 Photoluminescence properties

$NaY(MoO_4)_2$ shows excellent thermal and hydrolytic stability and is considered to be an effective luminescent host for rare earth ions to produce phosphors and laser crystals. Owing to the similar chemical properties of Y^{3+} and Eu^{3+}/Tb^{3+} ions [30], little doped Eu^{3+}/Tb^{3+} into $NaY(MoO_4)_2$ has no influence on the morphologies as shown in Fig. 5.

Figure 6 shows the PL excitation and emission spectra of the octahedron-like and rod-like $NaY(MoO_4)_2$:Eu^{3+} phosphors. The excitation spectra (Fig. 6, left) are obtained by monitoring the emission of the Eu^{3+} $^5D_0 \rightarrow {}^7F_2$ transition at 615 nm. The excitation spectra of $NaY(MoO_4)_2$:Eu^{3+} with different morphologies have similar profiles and each one consists of two parts. One part is a strong broad band ranging from 200 to 350 nm with a maximum at about 298 nm, which is attributed to the Mo^{6+}–O^{2-} and O^{2-}–Eu^{3+} charge transfer band. The other part in the excitation spectra is a series of sharp excitation peaks in the longer region (350–450 nm) associated with the general f–f transitions of Eu^{3+} ions. It is indicated that an energy transfer process occurs from the MoO_4^{2-} groups

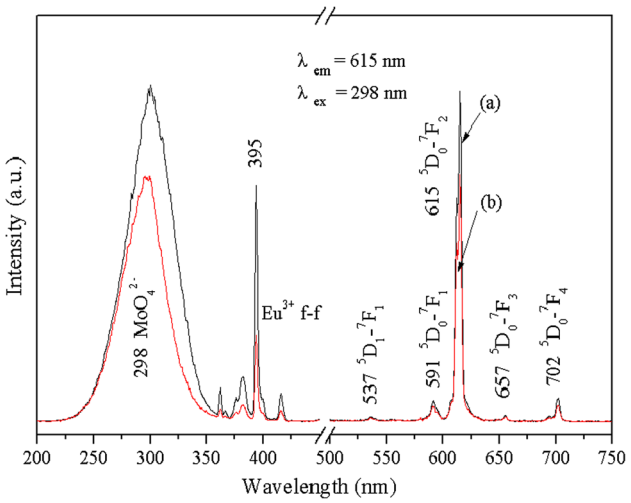

Fig. 6 Excitation and emission spectra of $NaY(MoO_4)_2$:Eu^{3+} samples with different morphologies: (*a*) octahedron-like microcrystals, (*b*) rod-like microcrystals

to Eu^{3+} ions in the crystal because of the presence of the excitation band of the MoO_4^{2-} groups in the excitation spectrum of Eu^{3+} ions. Upon excitation into the MoO_4^{2-} at 298 nm, the most intensive peak at 615 nm arises from the $^5D_0 \rightarrow {}^7F_2$ transition, while the other peaks at 537, 591, 657 and 702 nm correspond to the $^5D_1 \rightarrow {}^7F_1$, $^5D_0 \rightarrow {}^7F_1$, $^5D_0 \rightarrow {}^7F_3$, $^5D_0 \rightarrow {}^7F_4$ transitions of Eu^{3+} ions, respectively (Fig. 6, right). Moreover, according to Stark energy splitting [16], the (2 J + 1) Stark components of J-degeneracy splitting lead to the two subpeaks at 615 nm. The electric dipole transition $^5D_0 \rightarrow {}^7F_2$ is a hypersensitive transition and the emission intensity is strongly influenced by local environment surrounding Eu^{3+} ions. If Eu^{3+} is located at a low symmetry site, the $^5D_0 \rightarrow {}^7F_2$ transition should be dominant, while in a site with an inversion center, the $^5D_0 \rightarrow {}^7F_1$ magnetic dipole transition will be preponderant. In the present case, the emission intensity of $^5D_0 \rightarrow {}^7F_2$ is evidently stronger than the other one, which

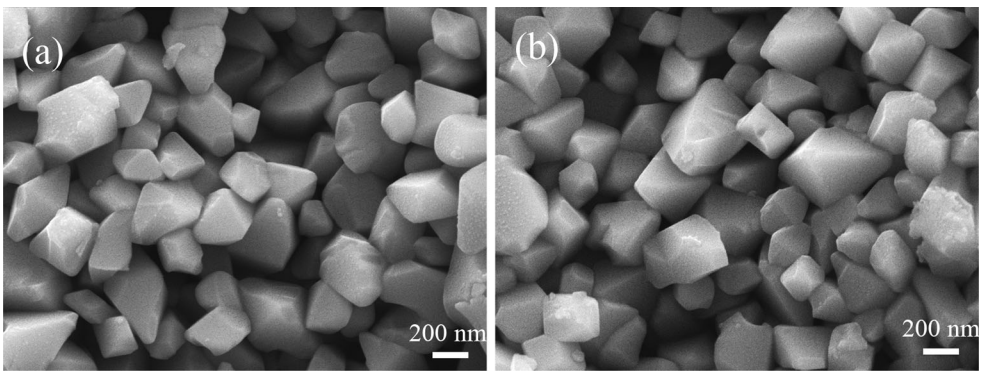

Fig. 5 FE-SEM images of Eu^{3+}/Tb^{3+} doped $NaY(MoO_4)_2$ obtained at 800 °C for 6 h: **a** $NaY(MoO_4)_2$:Eu^{3+} microcrystals, **b** $NaY(MoO_4)_2$:Tb^{3+} microcrystals

indicates that the non-inversion center site is occupied by Eu^{3+} in the $NaY(MoO_4)_2$ host lattice. Besides, the morphologies have no effect on the peak locations but can affect the red emission intensity strongly. And the PL intensity of octahedron-like microcrystals is stronger than the rod-like ones. It is believed that the improvement of the PL intensity may be attributed to the uniform morphology, average size and narrow particle size distribution.

The excitation spectra of the octahedron-like and rod-like $NaY(MoO_4)_2$:Tb^{3+} phosphors monitored with Tb^{3+} $^5D_4 \rightarrow {}^7F_5$ at 545 nm exhibit intensive and broad band from 200 to 350 nm peaked at 298 nm, which correspond to the charge-transform transitions within the MoO_4^{2-} groups (Fig. 7, left). The emission spectra consist of a group of lines centered at about 488, 545, 587, and 621 nm, which correspond to the $^5D_4 \rightarrow {}^7F_J$ (J = 6, 5, 4, 3) transitions of the Tb^{3+} ions, respectively (Fig. 7, right). By comparison of the emission spectra of $NaY(MoO_4)_2$:-Tb^{3+} with different morphologies, the emission intensity of the octahedron-like microcrystals is also stronger than the rod-like ones. The PL excitation of Tb^{3+} doped NaY $(MoO_4)_2$ crystals is much similar to that of the Eu^{3+} doped samples from 200 to 350 nm, implying that these samples can be rationally mixed for many practical applications due to their equal excitation wavelength.

The emission and energy transfer process in Eu^{3+} and Tb^{3+} doped $NaY(MoO_4)_2$ is shown schematically in Fig. 8a. Upon excitation at 298 nm, electrons of MoO_4^{2-} excite from the ground state to the highest state. Then the excited electrons either relax to the lowest vibrational level of the excited state of MoO_4^{2-}, or transfer non-radiatively to higher levels of Eu^{3+}, from which the energy relax to the $^5D_0$ or $^5D_1$ level by the cross-relaxation process (Fig. 8a, left). Red emission is obtained as a result of $^5D_1 \rightarrow {}^7F_1$ and $^5D_0 \rightarrow {}^7F_J$ (J = 1, 2, 3, 4) transitions. The excitation energy of MoO_4^{2-} is mainly transferred to the higher levels of Tb^{3+} (Fig. 8b, right). And the energy from the higher levels relaxes to $^5D_4$ level of Tb^{3+} by the same process compared with that of Eu^{3+}.

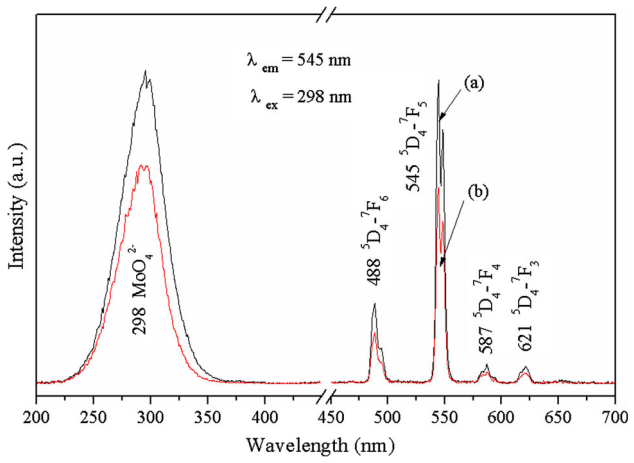

Fig. 7 Excitation and emission spectra of $NaY(MoO_4)_2$:Tb^{3+} samples with different morphologies: (*a*) octahedron-like microcrystals, (*b*) rod-like microcrystals

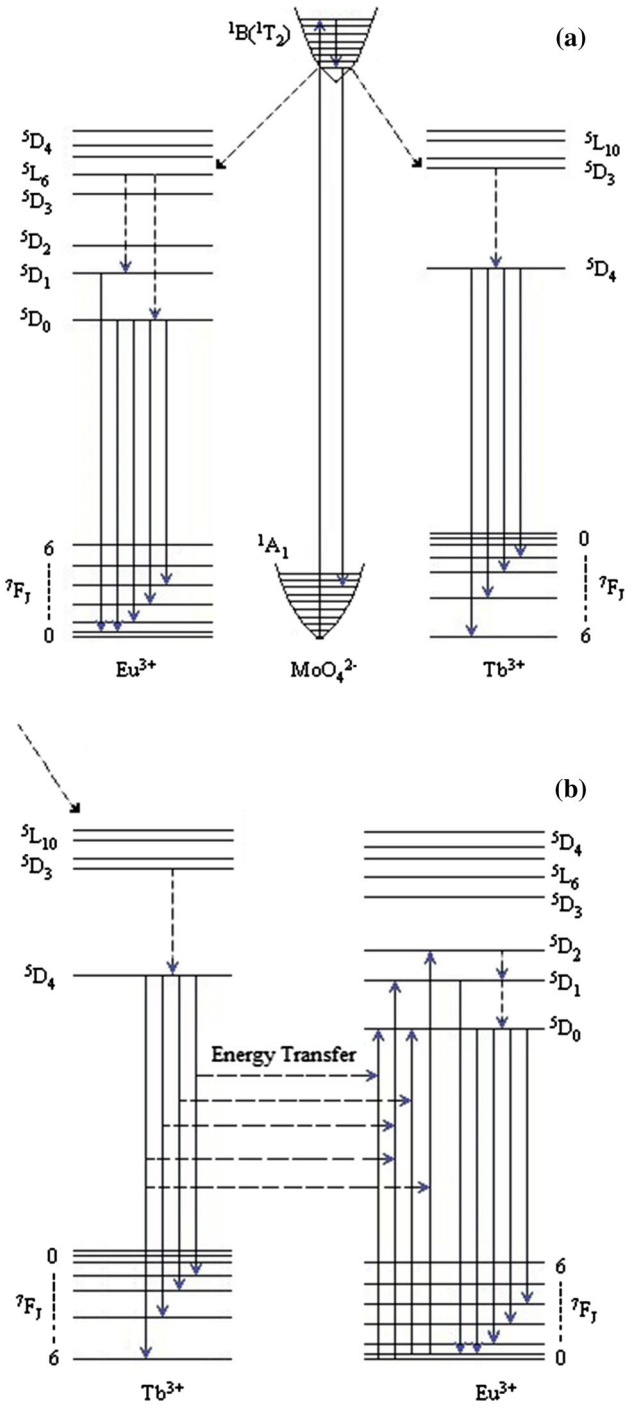

Fig. 8 Proposed energy transfer mechanisms: **a** from MoO_4^{2-} to Eu^{3+} and Tb^{3+}, **b** from Tb^{3+} to Eu^{3+}

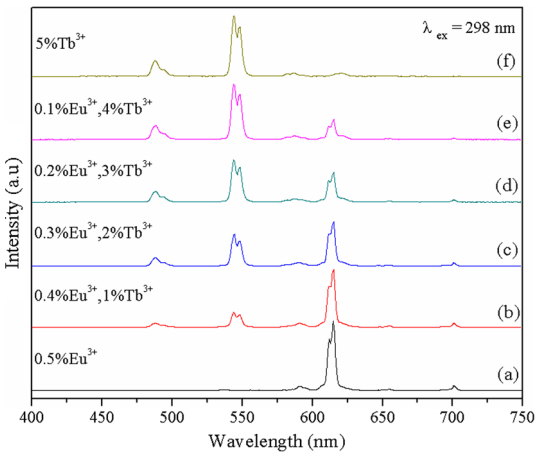

Fig. 9 Emission spectra of the Eu^{3+}–Tb^{3+} co-doped octahedron-like $NaY(MoO_4)_2$:xEu^{3+}, yTb^{3+} microcrystals

To investigate the tunable PL properties of the $NaY(MoO_4)_2$ crystals, we have co-doped Eu^{3+} and Tb^{3+} ions with different relative concentrations into the octahedron-like $NaY(MoO_4)_2$ host lattice, as the octahedron-like $NaY(MoO_4)_2$ give stronger emissions in the progress of this research. The emission spectra of the Eu^{3+}–Tb^{3+} co-doped $NaY(MoO_4)_2$ samples under the excitation at 298 nm are shown in Fig. 9. It can be seen that the as-prepared pure Eu^{3+}-doped $NaY(MoO_4)_2$ crystals show strong red emission under UV light excitation. With the doping of Tb^{3+} ions into the $NaY(MoO_4)_2$ host lattice, the characteristic emission of the Tb^{3+} ions can be found besides the Eu^{3+} emission. Green emissions gradually rise along with the increasing of Tb^{3+} concentration.

The emission and energy transfer process in Eu^{3+}–Tb^{3+} co-doped $NaY(MoO_4)_2$ is shown schematically in Fig. 8b. Firstly, electrons on MoO_4^{2-} relax to the higher levels of Tb^{3+} upon excitation at 298 nm. The electrons relax to the $^5D_4$ level, and then either return to the ground state to produce the Tb^{3+} emissions ($^5D_4$–$^7F_{6,\ 5,\ 4,\ 3}$), or transfer excitation energy from $^5D_4$ (Tb^{3+}) level to the higher excited energy levels of Eu^{3+} ($4f^6$) through cross relaxation, which relax to the $^5D_0$ or $^5D_1$ (Eu^{3+}) level, where the red emissions take place. The energy transfers from Tb^{3+} to Eu^{3+} could be very efficient due to large spectral overlap between Tb^{3+} emission and Eu^{3+} absorption [25].

The commission international Del'Eclairage (CIE) chromaticity coordinates of the Eu^{3+}–Tb^{3+} co-doped $NaY(MoO_4)_2$ phosphors was calculated based on the CIE 1931 standards (Table 1). The color of these samples can be tuned from red, orange, yellow and green-yellow to green by adjusting the associative doping ratio of Eu^{3+} and Tb^{3+} ions (Fig. 10, from a to f).This result indicates that the as-obtained phosphors could show merits of multicolor emissions in the visible region under UV light excitation,

Table 1 The CIE Chromaticity coordinates of the as-obtained Eu^{3+}–Tb^{3+} co-doped octahedron-like $NaY(MoO_4)_2$:xEu^{3+}, yTb^{3+} microcrystals: (a) 0.5 % Eu^{3+}, (b) 0.4 % Eu^{3+}, 1 % Tb^{3+}, (c) 0.3 % Eu^{3+}, 2 % Tb^{3+}, (d) 0.2 % Eu^{3+}, 3 % Tb^{3+}, (e) 0.1 % Eu^{3+}, 4 % Tb^{3+}, (f) 5 % Tb^{3+}

Coordinate	(a)	(b)	(c)	(d)	(e)	(f)
x	0.647	0.538	0.464	0.406	0.357	0.292
y	0.351	0.408	0.470	0.514	0.556	0.601

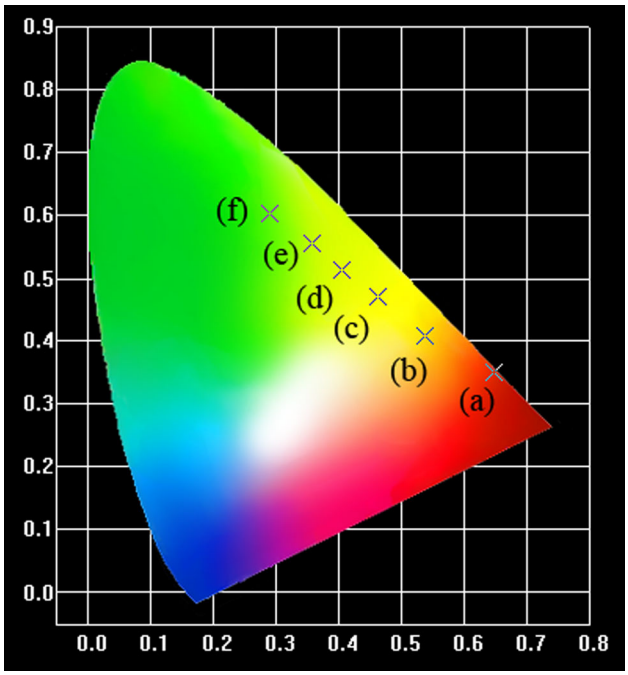

Fig. 10 CIE chromaticity diagram for the emission spectra of the as-obtained Eu^{3+}–Tb^{3+} co-doped octahedron-like $NaY(MoO_4)_2$:xEu^{3+}, yTb^{3+} microcrystals: (*a*) 0.5 % Eu^{3+}, (*b*) 0.4 % Eu^{3+}, 1 % Tb^{3+}, (*c*) 0.3 % Eu^{3+}, 2 % Tb^{3+}, (*d*) 0.2 % Eu^{3+}, 3 % Tb^{3+}, (*e*) 0.1 % Eu^{3+}, 4 % Tb^{3+}, (*f*) 5 % Tb^{3+}

which might make it possible that desired colors produced with $NaY(MoO_4)_2$ host lattice could have potential application in the areas such as optoelectronic devices in the future.

4 Conclusion

The $NaY(MoO_4)_2$ microcrystals with different morphologies have been synthesized with different reaction conditions via a low cost molten salt method. The calcining temperature and reaction time play critical roles in controlling the morphology and the size of the $NaY(MoO_4)_2$ samples. The octahedron-like crystals could be obtained at the calcining temperature of 800 °C for 6 h. The Eu^{3+}/Tb^{3+}

ions doped octahedron-like $NaY(MoO_4)_2$ phosphors show stronger red/green emission under UV light excitation than the rod-like ones. Moreover, when co-doping with Eu^{3+} and Tb^{3+} in an appropriate ratio, the PL emission colors of the $NaY(MoO_4)_2$:Eu^{3+}/Tb^{3+} phosphors can be tuned from red, orange, yellow and green-yellow to green, which might have potential application in the areas such as optoelectronic devices in the future.

Acknowledgments This work is financially supported by Priority Academic Program Development (PAPD) of Jiangsu Higher Education Institutions, Major Program for the Natural Scientific Research of Jiangsu Higher Education Institutions (12KJA430002) and Program for Changjiang Scholars and Innovative Research Team in University (PCSIRT), IRT1146.

References

1. H. Jung, D. Hwang, E. Kim, B.J. Kim, W.B. Lee, J.E. Poelma, J. Kim, C.J. Hawker, J. Huh, D. Ryu, J. Bang, ACS Nano **5**, 6164–6173 (2011)
2. C.T. Dinh, T.D. Nguyen, F. Kleitz, T.O. Do, ACS Nano **3**, 3737–3743 (2009)
3. Y. Tian, B. Chen, B. Tian, R. Hua, J. Sun, L. Cheng, H. Zhong, X. Li, J. Zhang, Y. Zheng, T. Yu, L. Huang, Q. Meng, J. Alloys Compd. **509**, 6096–6101 (2011)
4. J.C. Sczancoski, M.D.R. Bomio, L.S. Cavalcante, M.R.B. Joya, P.S. Pizani, J.A. Varela, E. Longo, M.S. Li, J.A. Andrés, J. Phys. Chem. C **113**, 5812–5822 (2009)
5. J. Thirumalai, R. Krishnan, I.B. Shameem Banu, R. Chandramohan, J. Mater. Sci.: Mater. Electron. **24**, 253–259 (2013)
6. B.K. Lim, M.J. Jiang, J. Tao, H.C. Camargo, Y.M. Zhu, Y.N. Xia, Adv. Funct. Mater. **19**, 189–200 (2009)
7. B.A. Marinkovic, M. Ari, R.R. de Avillez, F. Rizzo, F.F. Ferreira, K.J. Miller, M.B. Johnson, M.A. White, Chem. Mater. **21**, 2886–2894 (2009)
8. M.W. Stoltzfus, P.M. Woodward, R. Seshadri, J.H. Klepeis, B. Bursten, Inorg. Chem. **46**, 3839–3850 (2007)
9. R. Krishnan, J. Thirumalai, I.B. Shameem Banu, R. Chandramohan, J. Mater. Sci.: Mater. Electron. **24**, 4774–4781 (2013)
10. Y.H. Wang, Y.S. Liu, Q.B. Xiao, H.M. Zhu, R.F. Li, X.Y. Chen, Nanoscale **3**, 3164–3169 (2011)
11. C.X. Li, J. Lin, J. Mater. Chem. **20**, 6831–6847 (2010)
12. C. Bouzigues, T. Gacoin, A. Alexandrou, ACS Nano **5**, 8488–8505 (2011)
13. F. Yang, Y. Liu, Y. Lu, H. Chen, D. Zhang, H. Wu, J. Mater. Sci.: Mater. Electron. **25**, 3608–3613 (2014)
14. L. Armelao, S. Quici, F. Barigelletti, G. Accorsi, G. Bottaro, M. Cavazzini, E. Tondello, Coord. Chem. Rev. **254**, 487–505 (2010)
15. W. Bu, Y. Xu, N. Zhang, H. Chen, Z. Hua, J. Shi, Langmuir **23**, 9002–9007 (2007)
16. G.S. Yi, B.Q. Sun, F.Z. Yang, D.P. Chen, Y.X. Zhou, J. Cheng, Chem. Mater. **14**, 2910–2914 (2002)
17. G.H. Li, L.L. Li, M.M. Li, W.W. Bao, Y.H. Song, S.C. Gan, H.F. Zou, X.C. Xu, J. Alloys Compd. **550**, 1–8 (2013)
18. J. Liu, B. Xu, C. Song, H.D. Luo, X. Zou, L.X. Han, X.B. Yu, CrystEngComm **14**, 2936–2943 (2012)
19. Z.H. Xu, C.X. Li, G.G. Li, R.T. Chai, C. Peng, D.M. Yang, J. Lin, J. Phys. Chem. C **114**, 2573–2582 (2010)
20. Y. Huang, L.Q. Zhou, L. Yang, Z.W. Tang, Opt. Mater. **33**, 777–782 (2011)
21. X. Wang, L.S. Gao, F. Zhou, Z.D. Zhang, M.R. Ji, C.M. Tang, T. Shen, H.G. Zheng, J. Cryst. Growth **265**, 220–223 (2004)
22. L.J. Xie, J.F. Ma, J. Zhou, Z.Q. Zhao, H. Tian, Y.G. Wang, J.T. Tao, X.Y. Zhu, J. Am. Ceram. Soc. **89**, 1717–1720 (2006)
23. B. Yan, F. Lei, J. Alloys Compd. **507**, 460–464 (2010)
24. T. Wu, Y.F. Liu, Y.N. Lu, L. Wei, H. Gao, H. Chen, CrystEngComm **15**, 2761–2768 (2013)
25. Y. Zeng, Z. Li, L. Wang, Y. Xiong, CrystEngComm **14**, 7043–7048 (2012)
26. C.J. Mao, J. Geng, X.C. Wu, J.J. Zhu, J. Phys. Chem. C **114**, 1982–1988 (2010)
27. S.D. Hutagalung, *Materials Science and Technology, Materials Science* (InTech, Croatia, 2012)
28. Y. Li, G.F. Wang, K. Pan, W. Zhou, C. Wang, N.Y. Fan, Y.J. Chen, Q.M. Feng, B.B. Zhao, CrystEngComm **14**, 5015–5020 (2012)
29. J.F. Banfield, S.A. Welch, H.Z. Zhang, T.T. Ebert, R.L. Penn, Science **289**, 751–754 (2000)
30. L. Xu, X. Yang, Z. Zhai, X. Chao, Z. Zhang, W. Hou, Cryst EngComm **13**, 4921–4929 (2011)